Nanoscale

PAPER

View Article Online
View Journal | View Issue

Cite this: *Nanoscale*, 2019, **11**, 23475

Strong second-harmonic generation from Au–Al heterodimers†

Jiyong Wang, [a,b,c,d,e] Jérémy Butet,[f] Gabriel David Bernasconi,[f] Anne-Laure Baudrion, [b] Gaëtan Lévêque,[g] Andreas Horrer,[b,h] Anke Horneber, [a,c] Olivier J. F. Martin,[f] Alfred J. Meixner,[a,c] Monika Fleischer, [c,h] Pierre-Michel Adam*[b] and Dai Zhang *[a,c]

Second-harmonic generation (SHG) is investigated from three kinds of lithographically fabricated plasmonic systems: Al monomers, Au monomers and Au–Al heterodimers with nanogaps of 20 nm. Spectrally integrated SHG intensities and the linear optical responses are recorded and compared. The results show that for the monomer nanoantennas, the SHG signal depends sensitively on the linear excitation of the plasmon resonance by the fundamental wavelength. For Au–Al heterodimer nanoantennas, apart from fundamental resonant excitation, nonlinear optical factors such as SH driving fields and phase interferences need to be taken into account, which play significant roles at the excitation and scattering stages of SHG radiation. It is interesting to note that a possible energy transfer process could take place between the two constituting nanoparticles (NPs) in the Au–Al heterodimers. Excited at the linear plasmon resonance, the Au NP transfers the absorbed energy from the fundamental field to the nearby Al NP, which efficiently scatters SHG to the far-field, giving rise to an enhanced SHG intensity. The mechanisms reported here provide new approaches to boost the far-field SHG radiation by taking full advantage of strongly coupled plasmonic oscillations and the synergism from materials of different compositions.

Received 4th September 2019,
Accepted 12th November 2019

DOI: 10.1039/c9nr07644a

rsc.li/nanoscale

Introduction

Nonlinear optics was established shortly after the construction of the first laser system.[1] Nonlinear optical processes such as frequency-mixing,[2] optical Kerr effect,[3] optical phase conjugation,[4] four-wave mixing,[5] Raman amplification,[6] stimulated Brillouin scattering,[7] multi-photon absorption[8,9] and multiple photoionization[10] were systemically investigated in the last several decades. Their advanced applications range from optical fibers,[11] optical switches,[12] photonic crystals[13] and other optical devices to modern nanostructures. Compared to linear optical processes, the generation of nonlinear optical signals requires a much higher excitation field. Plasmonic nanoantennas can be used for the excitation of these optical processes since the field intensity at the fundamental wavelength is significantly enhanced in their vicinities thanks to the localized surface plasmon resonances (LSPRs).[8] LSPRs have indeed attracted particular attention as they allow enhancing and concentrating electromagnetic fields in sub-wavelength volumes.[14,15] Their influences on the nonlinear optical properties of plasmonic nanoantennas such as SHG,[8,16–20] two-photon photoluminescence (TPL),[9,21,22] third and higher harmonics generation,[23] as well as multi-photon photoluminescence[9] have been thoroughly investigated. Nonlinear plasmonics, as a new branch of nano optics, has emerged recently.[23]

Among different nonlinear optical processes, SHG has the advantage of being sensitive to the symmetry of plasmonic nanostructures as well as their spatial arrangement.[17,24–26] In order to achieve efficient SHG, different strategies are explored by taking linear and nonlinear optical factors into account. For

[a]*Institute of Physical and Theoretical Chemistry, Eberhard Karls University of Tübingen, Auf der Morgenstelle 15, 72076 Tübingen, Germany. E-mail: dai.zhang@uni-tuebingen.de*
[b]*Light, Nanomaterials and Nanotechnology, University of Technology of Troyes, 12 Rue Marie Curie, CS42060, 10004 Troyes Cedex, France. E-mail: pierre_michel.adam@utt.fr*
[c]*Center for Light-Matter-Interaction, Sensors and Analytics (LISA⁺), Eberhard Karls University of Tübingen, Auf der Morgenstelle 15, 72076 Tübingen, Germany*
[d]*Key Laboratory of 3D Micro/Nano Fabrication and Characterization of Zhejiang Province, School of Engineering, Westlake University, 18 Shilongshan Road, 310024 Hangzhou, Zhejiang Province, China*
[e]*Key Laboratory of 3D Micro/Nano Fabrication and Characterization of Zhejiang Province, School of Engineering, Westlake Institute for Advanced Study, 18 Shilongshan Road, 310024 Hangzhou, Zhejiang Province, China*
[f]*Nanophotonics and Metrology Laboratory (NAM), Swiss Federal Institute of Technology, Lausanne (EPFL), 1015 Lausanne, Switzerland*
[g]*Institut d'Electronique, de Microélectronique et de Nanotechnologie (IEMN, CNRS-8520), Cité Scientifique, Avenue Poincaré, 59652 Villeneuve d'Ascq, France*
[h]*Institute for Applied Physics, Eberhard Karls University of Tübingen, Auf der Morgenstelle 10, 72076 Tübingen, Germany*

†Electronic supplementary information (ESI) available. See DOI: 10.1039/c9nr07644a

instance, the design of nanostructures with non-centrosymmetric geometries becomes essential to obtain relatively high second order nonlinear susceptibility. Nanostructures with various shapes, such as split-ring resonators,[27] L-shaped NPs[28,29] and chiral G-shaped NPs[30] were designed for these purposes. Furthermore, when two isolated nanoantennas are close to each other, the near-field of one NP interacts with that of the adjacent one. Strongly-coupled plasmonic oscillations take place when the interdistance of the constituting NPs is small enough. The coupling effect can also lead to strong surface charge gradients at the separation gap, which dramatically enhances their individual optical response by many orders of magnitude.[31] These effects lead to many advanced applications involving gap antennas, bowtie antennas[32] and various nanodimers.[33] Benefiting from both advantages of asymmetry and nanogaps, a heterodimer which consists of two NPs with different materials becomes an attractive SHG emitter.[34]

In this article, SHG from Au and Al nanodiscs is systematically studied, since such materials allow the LSPRs of nanoantennas to be tailored either at the fundamental laser wavelength or at the SH wavelength.[35] Specifically, SHG from single Au disc monomers, Al disc monomers and Au–Al disc heterodimers with nanogaps is systematically investigated using a home-built scanning confocal nonlinear optical microscope, which is illustrated in the ESI.†[8,9,21,36] Spectrally integrated SHG intensities and the linear optical responses are recorded and compared experimentally. The corresponding theoretical simulations are performed with the assistance of a surface integral equation (SIE) method. The linear and nonlinear optical factors contributing to SHG radiation are analyzed for the three kinds of nanoantennas. Strategies to boost the far-field SHG radiation and design an efficient SHG emitter are explored.

Results

Three kinds of single plasmonic nanostructures are fabricated on glass slides using electron-beam lithography: Al disc monomers, Au disc monomers and Au–Al disc heterodimers. The disc diameter of the Al monomer varies from 120 nm to 200 nm with a step of 20 nm. The disc diameters of the Au monomer are 80 nm, 100 nm, 120 nm, 140 nm, 160 nm and 200 nm. The disc diameter of the Au and Al NPs in the Au–Al heterodimers is designed as 160 nm. The structure height is 50 nm. The spacing between the individual nanostructures is 10 μm such that the dark-field scattering measurements and the nonlinear optical measurements can be performed at a single NP level. All the nanostructures are fabricated on the same glass substrate using an overlay e-beam lithography technique. A femtosecond laser (~110 fs, 89 MHz, 774 nm, TEM00 Gaussian mode) is employed in a home-built scanning confocal optical microscope to excite the sample, and only the nonlinear optical signals are collected. A detailed description of the fabrication procedure as well as the setups used for the linear and nonlinear optical measurements can be found in the ESI.† For simplification, the abbreviations "Ald1", "Aud2" are used to represent the Al monomer with the disc diameter of "d1" nm and the Au monomer with the disc diameter of "d2" nm, respectively. "Aud1-Ald1-Gd2" represents an Au–Al heterodimer, which comprises a Au NP and an Al NP with the disc diameters of "d1" nm. The edge-to-edge gap size G is "d2" nm.

In Fig. 1, SEM images (a–c), spectrally integrated optical images (d–f) and normalized emission spectra (g–i) of an Al160 nanodisc (a, d and g), a Au160 nanodisc (b, e and h) and a Au160-Al160-G20 heterodimer (c, f and i) are given as examples of the fabricated nanostructures and their corresponding nonlinear optical responses. The intensities of the optical images are derived from the nonlinear spectra which are spectrally integrated from 370 nm to 680 nm. For the heterodimers, the incident beam is linearly polarized along the long dimer axis (see Fig. S2 in ESI† for polarization dependent SHG from Au160–Al160 heterodimers). A narrow peak situated at 387 nm is observed in the emission spectra, which corresponds to SHG (highlighted by the violet background). The width of the SHG peak is related to the bandwidth of the femtosecond laser pulses. In the following analysis, the intensity integrated from 380 nm to 390 nm is used for analyzing the SHG signal. A broad peak, with a maximum at longer wavelengths than the SH peak, corresponds to the TPL signal,

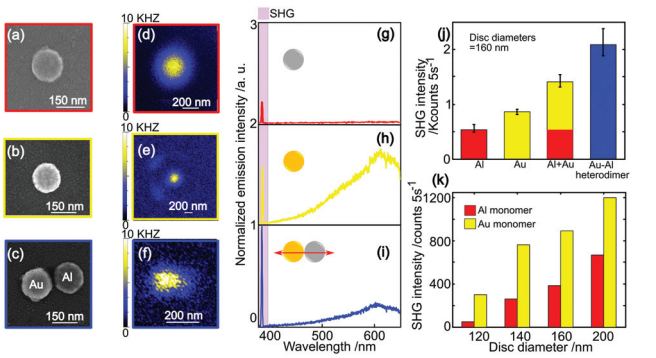

Fig. 1 The SEM images (a–c), nonlinear optical images (d–f) and emission spectra (g–i) of a single Al160 nanodisc (a, d and g), Au160 nanodisc (b, e and h) and Au160-Al160-G20 heterodimer (c, f and i). The scale bars in the SEM images and nonlinear optical images represent 150 nm and 200 nm, respectively. Optical images (d–f) are spectrally integrated from 370 nm to 680 nm and comprise the sum of the SHG-signal and part of the TPL-signal which is the broad band with a maximum at 610 nm. The peaks appearing at 387 nm in the nonlinear optical spectra (g–i) represent the SHG signals, which are highlighted by the violet background. For a better comparison of the SHG intensity in (g–i), the SHG peak shown in (i) is regarded as 1 relative to which the SHG peaks in (g) and (h) are normalized. (j) Spectrally integrated SHG intensities are compared among a single Al160 monomer (red), a Au160 monomer (yellow), the sum of an Al160 monomer and a Au160 monomer, as well as a Au160-Al160-G20 heterodimer (blue). The error bars represent different measurements for the same size of nanoantennas. (k) Spectrally integrated SHG intensities are compared between single Al monomers (red) and Au monomers (yellow) with the same disc diameters. The SHG intensities are spectrally integrated from 380 nm to 390 nm.

which shows a second order dependence (see Fig. S3 in ESI†) on the excitation laser power. Notably, Al monomers show barely any TPL signal in the experiment, as seen in Fig. 1(g).

Spectrally integrated SHG emission intensities are first compared for different systems with the same disc diameter. As shown in Fig. 1(j), SHG emission intensities are compared between an Al160 monomer (red), a Au160 monomer (yellow) and a Au160-Al160-G20 heterodimer (blue). The Al monomer has the weakest intensity, while the heterodimer has the strongest. The SHG intensity from the heterodimer is even stronger than the sum of those of the individual Au and Al NPs.

A further comparison is made between the Au and Al monomer systems. As shown in Fig. 1(k), spectrally integrated SHG emission intensities are compared for Al monomers (red) and Au monomers (yellow) with the same disc diameters. SHG from both Al and Au monomers increases as the disc diameter evolves from 120 nm to 200 nm. In the meantime, it can be clearly seen that Au monomers emit much stronger SHG than the Al monomers for each disc diameter.

Discussion

Due to the selection rules of the second order nonlinear susceptibility tensor χ^2, SHG from the bulk of centrosymmetric materials is forbidden in the electric dipole approximation. This selection rule needs to be relaxed for the observation of SHG. For example, surfaces can generate SHG, since the centrosymmetry is broken at the material interfaces considering the finite dimension of atom lattices. This is notably the case for plasmonic nanostructures. As has been reported, the component $\chi_{\mathrm{surf},\perp\perp\perp}$ (where $\perp$ denotes the component normal to the surface) of the surface tensor creates the dominant contribution for SHG from plasmonic nanostructures.[8,24] Other contributions, such as the tangential component of the surface tensor as well as bulk contributions, contribute only weakly to the total SH response. The local nonlinear polarization can thus be written as:[18]

$$P_{\mathrm{surf},\perp}(r,2\omega) = \chi_{\mathrm{surf},\perp\perp\perp}\, E_{\mathrm{n}}(r,\omega)E_{\mathrm{n}}(r,\omega) \quad (1)$$

From the above equation, the possible reasons for which the Au–Al heterodimer radiates the strongest SHG might be: (a) a particularly high local field enhanced by the coupling between individual single NPs; (b) a high asymmetry in the nanogap induces a greater component $\chi_{\mathrm{surf},\perp\perp\perp}$.

Monomers

Al NPs normally have a greater value of $\chi_{\mathrm{surf},\perp\perp\perp}$ than Au.[1,37] For instance, at the pump wavelength of 800 nm $\chi_{\mathrm{surf},\perp\perp\perp}$ of Al is more than ten times larger than that of Au.[1] Therefore, the reason that Au NPs have higher SHG than Al NPs shown in Fig. 1(k) can be attributed to a higher electric field enhancement induced by LSPRs. Indeed, compared to linear optical processes, the generation of nonlinear optical signals requires a much higher excitation field. The conversion yield of nonlinear optical processes is expected to increase with the fourth (for second order processes) or a higher power with the local field factor evaluated at the fundamental frequency.[8] Therefore, the local field enhancement should be the predominant factor for understanding the SHG radiation from monomer nanoantennas shown in the Fig. 1.

The high local electric field enhancement at the plasmonic nanostructure is closely related to its LSPRs. To characterize their properties, the linear optical responses are measured using a dark-field scattering microscope at the single particle level. The corresponding simulations are performed by using the SIE method (see ESI† for more details).

Fig. 2(a) and (c) show experimental and simulated dark-field scattering spectra from the single Al monomers, respectively. The maxima of the experimental dark-field scattering spectra of Al monomers shift from 480 nm to 580 nm (from 420 nm to 620 nm in simulation) as the disc diameter increases from 120 nm to 200 nm. The FWHM in both experiment and simulation increases with the disc diameter.

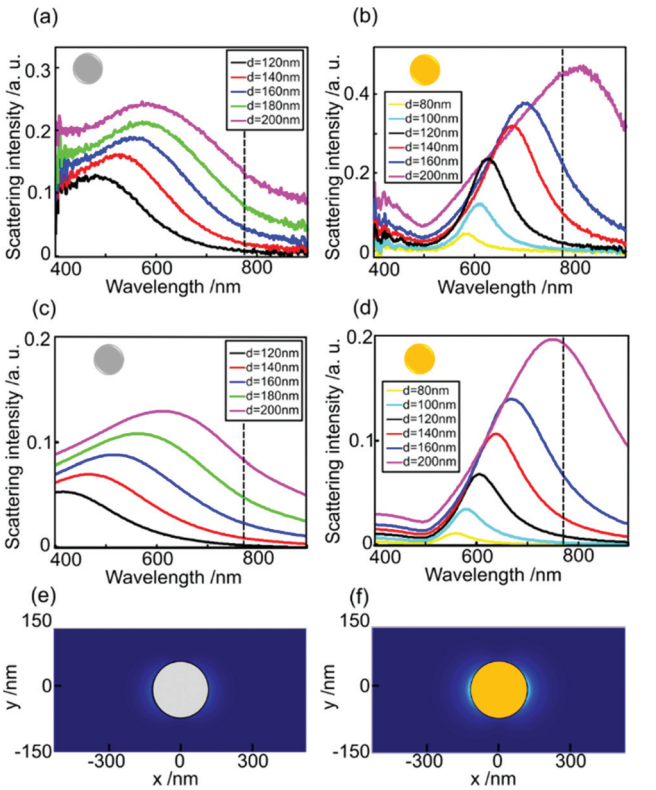

Fig. 2 (a) and (c) show the experimental and simulated dark-field scattering spectra from the single Al monomers, respectively. The disc diameter of the Al monomers varies from 120 nm (black), 140 nm (red), 160 nm (blue), 180 nm (green) to 200 nm (magenta). (b) and (d) show the experimental and simulated dark-field scattering spectra from the single Au monomers, respectively. The disc diameter of the Au monomers changes from 80 nm (yellow), 100 nm (cyan), 120 nm (black), 140 nm (red), 160 nm (blue) to 200 nm (magenta). The vertical black dashed lines represent the fundamental excitation wavelength: 774 nm. (e) and (f) show simulated near-field distributions of the Al160 monomer and Au160 monomer at the fundamental frequency by using the same color scale.

Fig. 2(b) and (d) shows the experimental and simulated dark-field scattering spectra from the single Au monomers, respectively. The peak position of the experimental dark-field scattering spectra of Au monomers shifts from 580 nm to 810 nm (from 560 nm to 740 nm in simulation) as the disc diameter increases from 80 nm to 200 nm.

The SHG intensity differences observed in Fig. 1(k) can be interpreted by considering the local field enhancement supported by the LSPRs. The light–matter interaction can be simplified by using a classical Lorentzian oscillator model. The closer the LSPR is with respect to the excitation frequency, the more energy can be transferred. The sharper the spectral linewidth, the less dephasing is involved, which induces a more efficient excitation by the driving field.[38] As can be seen from Fig. 2(a–d), the LSPRs of Au monomers have sharper linewidths and are closer to the fundamental excitation wavelength, compared to the Al monomers of the same size. This induces a stronger local field at the fundamental frequency, as shown in Fig. 2(e) and (f). Consequently, SHG radiated from the monomer nanoantennas strongly depends on the resonant excitation condition.

The resonant excitation at the fundamental frequency can be quantified by using an unperturbed Lorentzian oscillator.[38–40] The resonant excitation factor (REF) is defined here to analyze the influence of LSPRs on the radiation of SHG:

$$\mathrm{REF}(\omega,\gamma) = (\gamma/2\pi)/[(\omega-\omega_0)^2 + (\gamma/2)^2] \quad (2)$$

where ω_0 denotes the fundamental driving frequency, ω represents the resonance frequency of the plasmonic nanostructure, and γ describes the system damping. Notably, $\gamma = \gamma_0 + \Delta\gamma$. The term γ_0 denotes the damping constant of free electrons, which is determined by the material properties. According to the literature, $\hbar\gamma_0$ equals 128.7 meV and 70.88 meV for bulk Al and Au.[41] $\Delta\gamma$ denotes the lifetime of the plasmonic mode, which is described by the resonance FWHM. When the spectral linewidth broadening is neglected, the resonance profile will approach a delta function.[40] In this case, $\Delta\gamma$ approaches zero, and the system damping is only determined by the material properties.[42]

In the following analysis the resonance frequencies and FWHMs are extracted from the experimental scattering spectra, and the REFs are calculated in accordance with eqn (2). The trends of the calculated REFs are compared with the experimental and theoretical SHG intensities for the two plasmonic systems: Al monomers (Fig. 3(a)) and Au monomers (Fig. 3(b)). For a better illustration, the REFs, experimental and theoretical values are independently normalized to the respective maximum values observed among the monomers for each method. As can be seen in Fig. 3, the influence of REFs on the SHG intensity observed from NPs of different diameters reflects the experimental observation, and its behavior fits well with the prediction by the SIE method. As expected, a stronger influence of the REF is observed for the Au monomers. As the disc diameter increases, the LSPRs of Al and Au monomers

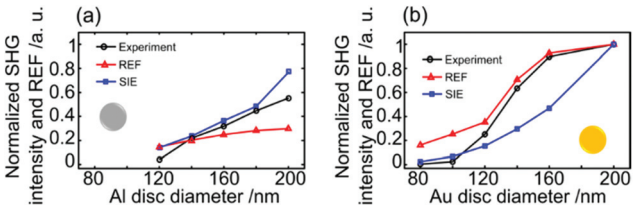

Fig. 3 The diameter-dependences of the normalized calculated REFs (red triangles) are compared with the normalized experimental SHG intensities (black circles) and theoretical SHG (blue squares) in Al monomers (a) and Au monomers (b).

shift towards the fundamental wavelength, giving rise to a stronger SHG radiation. The red-shifts are so dominant for Au monomers with increasing disc diameter that the resonance broadening does not impact the REF dramatically, in comparison with Al monomers. Thus, stronger SHG can be obtained as the disc diameter increases from 80 nm to 200 nm. The slight deviation between the REFs and theoretical results in the monomer systems in Fig. 3 might be due to a red shift of the plasmon resonance for the larger Al monomers and a blue shift of the plasmon resonance for the Au monomers in the theoretical calculations compared to the measured spectra, as seen in Fig. 2(a–d).

Heterodimers

SHG radiation from a coupled heterodimer system cannot be simply predicted by using the unperturbed Lorentzian oscillator model. The possible reasons are: (a) more than one resonances are involved in a dimer system; (b) new resonances different from the isolated single NPs can be generated due to the coupling effect; (c) higher order driving fields, *e.g.* SH sources in the vicinity of the NP, become non-negligible. More complicated nonlinear optical factors such as the phase interference should be considered as well. The fundamental and SH driving fields and optical phase interferences at the SH frequency will be analyzed in the following discussion.

First of all, the fundamental driving field that is strongly supported by LSPRs of nanoantennas is considered. Fig. 4(a) and (b) shows the experimental and simulated scattering spectra from a single Au160-Al160-G20 heterodimer, respectively. The excitation polarization is along the long dimer axis. The scattering spectra of the heterodimer show more than one single coupled plasmon mode. The eigenmodes of the plasmons are analyzed theoretically. Real and imaginary parts of the surface charges of two plasmon modes in the heterodimer are shown in the insets of Fig. 4(b).

The first one, which appears around 560 nm, behaves as a quadrupolar–quadrupolar-like coupled plasmon mode, and the second one, which is situated around 760 nm, is the dipolar–dipolar coupled plasmon mode. As the second coupled mode at 760 nm is much closer to the fundamental excitation, in comparison with Al160 and Au160 monomers, this could be one of the reasons for which the Au–Al heterodimer has the strongest SHG radiation in the far field, as shown

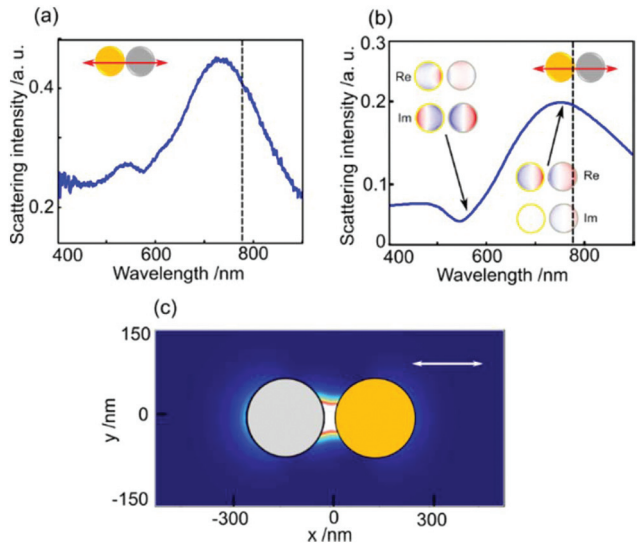

Fig. 4 (a) and (b) show the experimental and simulated scattering spectra from the single Au160-Al160-G20 heterodimer, respectively. The insets show the real and imaginary parts of the surface charges of two plasmon modes. The vertical black dashed lines represent the fundamental excitation wavelength: 774 nm. (c) Shows the near-field distribution of the Au160-Al160-G20 heterodimer at the fundamental frequency, using the same color scale as Fig. 2(e and f). The red and white arrows denote the excitation polarization. The excitation polarization is along the long dimer axis.

in Fig. 1(j). Strong electric field enhancements can be observed at the 'hot spot' in the nanogap when the excitation polarization is along the long axis of the heterodimer, as shown in Fig. 4(c).

Apart from the fundamental field, the SH driving field from adjacent NPs in a heterodimer system is also considered. As shown in Fig. 5(a) and (b), near-field SH electric field distributions of a Au160-Al160-G20 heterodimer are computed with the SIE method, by positioning the SH sources at the Al NP and Au NP, respectively. Interestingly, when the sources are at the Al NP, only weak SHG signal is generated from the Au NP, as seen in Fig. 5(a). This could be explained by the fact that interband transitions of Au severely dampen SHG when the excitation wavelength is less than 500 nm.[39] Nevertheless, as can be seen from Fig. 5(b), the Al NP can be efficiently driven by the SH sources coming from the Au NP, since small interband absorption effects of Al are encountered only at around 800 nm.[34] That SHG can be driven by the SH electric field of an adjacent NP offers further evidence why a heterodimer emits stronger SHG than the sum of the individuals. When SH sources are located on both NPs, as shown in Fig. 5(c), the hot spots at the SH frequency appear in the nanogap while the excitation polarization is along the dimer long axis. The strong localized SH fields are induced not only by the coupling effect at the fundamental frequency, but also by a 'synergy effect' of two constituting NPs at the SH frequency. Resonant excitation enables Au NPs to enhance and thus convert more fundamental field into energy at the SH frequency in comparison with the Al NP. The Au NP, however, cannot radiate SHG as efficiently as the Al NP at the SH frequency due to the interband transitions in Au. This 'synergy effect' creates a way that the Au NP transfers the resonantly absorbed energy to the Al NP, and the Al NP efficiently emits SH radiation. This could be one of the reasons for such a symmetry breaking system to increase the conversion yield of SHG processes.

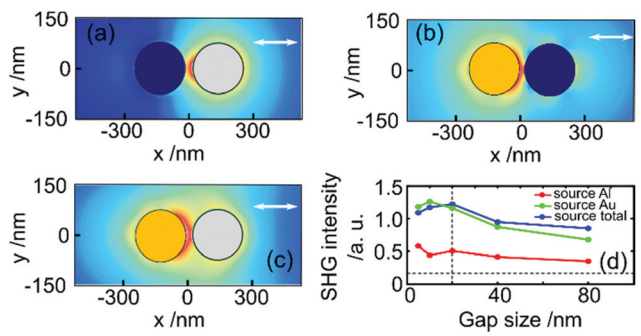

Fig. 5 (a)–(c) Near-field SH electric field distributions of a Au160-Al160-G20 heterodimer when SH sources are placed at the Al NP (right NP), Au NP (left NP), and both NPs, respectively. The color scales are kept the same as Fig. 2(e, f) and 4(c). (d) Far-field SHG intensities of Au160–Al160 heterodimers as a function of gap size. SHG intensities are calculated when SH sources are located at the Al NP (red), Au NP (green) and both NPs (blue), respectively. The excitation polarization is along the dimer long axis.

Furthermore, phase interference is another important factor when considering the propagation of the SHG light to the far-field. As shown in Fig. 5(d), far-field SHG intensities of Au160–Al160 heterodimers as a function of gap size are calculated when SH sources are located at the Al NP, Au NP, and both NPs. When the gap is less than 20 nm (vertical dashed line), SHG intensities with sources at both NPs are even smaller than the cases with sources at only Au NPs. This phenomenon has been reported as the 'silencing' of the second order nonlinear response.[8,20,43,44] Although a strong near-field enhancement is present, the nonlinear polarization vectors at each side of the gap are out of phase and their contributions to the far-field SH wave tend to cancel each other out.[43,44] The destructive interference finally results in a limited far-field SH signal, despite the amplitude of the nonlinear surface polarization. When the gap size increases, far-field SHG intensity from a heterodimer decreases exponentially.[31] For an infinitive gap size, the heterodimer turns into two isolated NPs, and SHG radiation ideally will approach the sum of two individuals (horizontal dashed line).[45] This appears straightforward, considering the gradual absence of plasmonic coupling effects (see Fig. S4 in ESI† for direct comparison of SHG intensity between the experimental results and calculated results).

Conclusions

Far-field SHG radiation from Al monomers, Au monomers and Au–Al heterodimers with nanogaps are systematically investi-

gated and compared in terms of experiments and numerical calculations in this study. Linear and nonlinear optical factors involved in the process of SHG are analyzed for each kind of nanoantenna system. Results show that for the monomer nanoantennas, SHG radiation has a strong dependence on the resonant excitation condition, where the localized fundamental electric field offered by plasmonic resonances plays a predominant role. Regarding Au–Al heterodimer nanoantennas, both linear and nonlinear optical factors need to be considered. The linear factor is mainly determined by the resonant excitation condition due to the coupled plasmonic resonances. Nonlinear optical factors such as the electric field at the SH frequency and phase interferences play important roles at the excitation and scattering stages of SHG radiation. The study also finds that the two constituting NPs of a Au–Al heterodimer respond distinctly differently to SH sources in their vicinities. In a synergistic system, the Au NP serves as an efficient absorber at the fundamental frequency and thus converter to SH near-fields, whereas the Al NP acts as an efficient SH emitter. These results provide new insights into the nonlinear optical properties of complex plasmonic systems, and the strategies to enhance the far-field SHG radiation from the aspects of linear and nonlinear optical factors. It offers a brief but useful guide to design efficient SHG emitters for the development of new applications in nonlinear plasmonics.

Conflicts of interest

There are no conflicts to declare.

Acknowledgements

Financial support from the Deutscher Akademischer Austauschdienst (DAAD), the Institutional Strategy of the University of Tübingen (Deutsche Forschungsgemeinschaft, ZUK 63), the Conseil Regional of Champagne-Ardennes and the Fonds Européens de Développement Régional (FEDER) through the use of the Nanomat platform. National Natural Science Foundation of China (NSFC, no. 61905200), the Swiss National Science Foundation (project200020_153662) and PHC PROCOPE (PROJET N° 30755YA) are gratefully acknowledged. J. Y. W. also acknowledges the support from Chinese scholarship council (CSC).

References

1 J. Butet, P.-F. Brevet and O. J. Martin, *ACS Nano*, 2015, **9**, 10545.
2 M. Danckwerts and L. Novotny, *Phys. Rev. Lett.*, 2007, **98**, 026104.
3 J. Porto, L. Martin-Moreno and F. Garcia-Vidal, *Phys. Rev. B: Condens. Matter Mater. Phys.*, 2004, **70**, 081402.
4 P.-Y. Chen and A. Alù, *Nano Lett.*, 2011, **11**, 5514.
5 L. Deng, E. W. Hagley, J. Wen, M. Trippenbach, Y. Band, P. S. Julienne, J. Simsarian, K. Helmerson, S. Rolston and W. D. Phillips, *Nature*, 1999, **398**, 218.
6 W. Cheng, Y. Avitzour, Y. Ping, S. Suckewer, N. J. Fisch, M. S. Hur and J. S. Wurtele, *Phys. Rev. Lett.*, 2005, **94**, 045003.
7 Z. Zhu, D. J. Gauthier and R. W. Boyd, *Science*, 2007, **318**, 1748.
8 J. Wang, J. Butet, A.-L. Baudrion, A. Horrer, G. Lévêque, O. J. Martin, A. J. Meixner, M. Fleischer, P.-M. Adam, A. Horneber and D. Zhang, *J. Phys. Chem. C*, 2016, **120**, 17699.
9 J. Wang, E. Gürdal, A. Horrer, S. Dickreuter, S. Kostcheev, A. J. Meixner, M. Fleischer, P.-M. Adam and D. Zhang, *Nanoscale*, 2018, **10**, 8240.
10 J. Eberly, Q. Su and J. Javanainen, *Phys. Rev. Lett.*, 1989, **62**, 881.
11 N. Broderick, T. Monro, P. Bennett and D. Richardson, *Opt. Lett.*, 1999, **24**, 1395.
12 S. Friberg and P. Smith, *IEEE J. Quantum Electron.*, 1987, **23**, 2089.
13 P. Russell, *Science*, 2003, **299**, 358.
14 W. L. Barnes, A. Dereux and T. W. Ebbesen, *Nature*, 2003, **424**, 824.
15 L. Novotny and N. Van Hulst, *Nat. Photonics*, 2011, **5**, 83.
16 J. Butet, J. Duboisset, G. Bachelier, I. Russier-Antoine, E. Benichou, C. Jonin and P.-F. Brevet, *Nano Lett.*, 2010, **10**, 1717.
17 J. Butet, K. Thyagarajan and O. J. Martin, *Nano Lett.*, 2013, **13**, 1787.
18 J. Butet and O. J. Martin, *ACS Nano*, 2014, **8**, 4931.
19 C. Dreser, A. Gollmer, X. Zang, D. P. Kern, M. Kauranen and M. Fleischer, *Nanoscale*, 2019, **11**, 5429.
20 G. Bautista, C. Dreser, X. Zang, D. P. Kern, M. Kauranen and M. Fleischer, *Nano Lett.*, 2018, **18**, 2571.
21 A. Horneber, F. Wackenhut, K. Braun, X. Wang, J. Wang, D. Zhang and A. J. Meixner, *Appl. Phys. B: Lasers Opt.*, 2017, **123**, 49.
22 G. Hajisalem, M. S. Nezami and R. Gordon, *Nano Lett.*, 2014, **14**, 6651.
23 M. Kauranen and A. V. Zayats, *Nat. Photonics*, 2012, **6**, 737.
24 G. Bachelier, J. Butet, I. Russier-Antoine, C. Jonin, E. Benichou and P.-F. Brevet, *Phys. Rev. B: Condens. Matter Mater. Phys.*, 2010, **82**, 235403.
25 Z.-J. Yang, Q. Zhao, Y.-H. Deng, D. Zhang and J. He, *Opt. Express*, 2018, **26**, 5835.
26 S.-J. Ding, H. Zhang, D.-J. Yang, Y.-H. Qiu, F. Nan, Z.-J. Yang, J. Wang, Q.-Q. Wang and H.-Q. Lin, *Nano Lett.*, 2019, **19**, 2005.
27 S. Linden, F. Niesler, J. Förstner, Y. Grynko, T. Meier and M. Wegener, *Phys. Rev. Lett.*, 2012, **109**, 015502.
28 S. Kujala, B. K. Canfield, M. Kauranen, Y. Svirko and J. Turunen, *Phys. Rev. Lett.*, 2007, **98**, 167403.
29 M. Baselli, A.-L. Baudrion, L. Ghirardini, G. Pellegrini, E. Sakat, L. Carletti, A. Locatelli, C. De Angelis, P. Biagioni, L. Duo, M. Finazzi, P.-M. Adam and M. Celebrano, *Plasmonics*, 2017, **12**, 1595.

30 V. Valev, N. Smisdom, A. Silhanek, B. De Clercq, W. Gillijns, M. Ameloot, V. Moshchalkov and T. Verbiest, *Nano Lett.*, 2009, **9**, 3945.
31 P. K. Jain, W. Huang and M. A. El-Sayed, *Nano Lett.*, 2007, **7**, 2080.
32 F. Laible, D. A. Gollmer, S. Dickreuter, D. P. Kern and M. Fleischer, *Nanoscale*, 2018, **10**, 14915.
33 S. Dickreuter, D. P. Kern and M. Fleischer, *Nanophotonics*, 2018, **7**, 1317.
34 A. Horneber, A.-L. Baudrion, P.-M. Adam, A. J. Meixner and D. Zhang, *Phys. Chem. Chem. Phys.*, 2013, **15**, 8031.
35 K.-Y. Yang, J. Butet, C. Yan, G. D. Bernasconi and O. J. F. Martin, *ACS Photonics*, 2017, **4**, 1522.
36 M. Lieb and A. Meixner, *Opt. Express*, 2001, **8**, 458.
37 M. Castro-Lopez, D. Brinks, R. Sapienza and N. F. van Hulst, *Nano Lett.*, 2011, **11**, 4674.
38 R. E. Blake, *Basic vibration theory*, McGraw-Hill Professional Publishing, New York, USA, 1961.
39 B. Metzger, M. Hentschel and H. Giessen, *ACS Photonics*, 2016, **3**, 1336.
40 W. Demtröder, *Laser spectroscopy: basic concepts and instrumentation*, Springer Science & Business Media, Berlin, Germany, 2013.
41 E. J. Zeman and G. C. Schatz, *J. Phys. Chem.*, 1987, **91**, 634.
42 B. Gallinet, T. Siegfried, H. Sigg, P. Nordlander and O. J. F. Martin, *Nano Lett.*, 2013, **13**, 497.
43 J. Berthelot, G. Bachelier, M. Song, P. Rai, G. C. Des Francs, A. Dereux and A. Bouhelier, *Opt. Express*, 2012, **20**, 10498.
44 S.-D. Liu, P. Yue, M.-Q. Zhu, J. Wen and D. Lei, *Opt. Express*, 2019, **27**, 26377.
45 J. Butet, G. D. Bernasconi and O. J. F. Martin, *Beilstein J. Nanotechnol.*, 2018, **9**, 2674.